Micro-Raman spectroscopy of the solid state: applications to semiconductors and thin films

T. Jawhari

Serveis Científico-Tècnics, Universitat de Barcelona, 08028 Barcelona, Spain

The potential of Raman microspectroscopy as a powerful tool in characterizing solids will be demonstrated here with several applications on semiconductors and thin films. The method not only permits the identification of different localized microscopic regions, with a high spatial resolution and with no sample preparation, but also provides several basic information on the microstructure of solids.

Introduction

In this article, we will analyze the possibilities that offer the micro-Raman method in the field of the solid state. Most of the examples that we shall here present are related to semiconducting materials and thin films. The characterization of these materials has clearly benefited from the advances that took place in Raman microscopy during the last two decades. The micro-Raman method is now recognized as a powerful and versatile tool for the analysis of solid films and condensed matter in general with its main feature being the chemical sensitivity. Furthermore, the Raman signal is also very sensitive to the microstructural state and other local environments of solids providing therefore information on the structure of the material on the scale of a few lattice constants. Raman signal is a function of the electron-phonon interaction, *i.e.* lattice vibration, and is a good complementary method to other techniques used in the characterization of the solid state such as transmission electron microscopy (TEM), X-rays diffraction, X-ray photoelectron spectroscopy (XPS), secondary ion mass spectroscopy (SIMS), Auger electron spectroscopy, etc. The micro-Raman technique has several fundamental advantages that are precious when studying solids:

– First of all, the method is contactless and therefore allows non destructive and quantitative microanalysis of structural and electrical properties. No sample preparation is required, which is a crucial point when characterizing processed devices, whereas most of the other techniques cited above involve a special preparation of the samples which may alter their structural properties.

– The high spatial resolution obtained with the Raman microscope is another fundamental benefit that allows to probe smaller dimensional scale devices. This is important for the analysis of microstructures and devices, where the properties of the layers are strongly process dependent and may differ significantly from the bulk material properties.

– Further, most of the semiconducting materials are quite opaque to visible light hence the high power density that is obtained with the Raman microprobe gives better results than the classical macro-Raman system.

Therefore, the micro-Raman system is now one of the preferred methods when characterizing semiconducting materials and thin films.

Instrumentation

All the Raman spectra presented here where obtained in the *Serveis Científico-Tècnics* of the University of Barcelona in collaboration with the Department of Electronics and the Department of Applied Physics and Optics. The micro-Raman instrument used to record these spectra is the T64000 of Jobin Yvon which consists in a typical optical microscope from Olympus combined with a triple monochromador dispersive system and a CCD detector cooled at liquid nitrogen temperature. The excitation source was produced by an Argon Ion laser at 514.5 nm. The laser power was usually low, *i.e.* about 1-2 mW at sample, in order to avoid any transformation in the structure of the samples.

Raman analysis of solids

In this part we will briefly review the different types of information on the microstructure and physical parameters of the condensed matter that can be obtained from the Raman spectrum.

Frequency

The frequency of the phonon Raman band depends on the masses and positions of the atoms, the interatomic forces (*i.e.* force constants of the bonds) and the bond length. Therefore, any effects altering these features will produce a

Article available at http://analusis.edpsciences.org or http://dx.doi.org/10.1051/analusis:2000280015

change in the frequency of the band. For instance, this is the reason why the band position is sensitive to the presence of stresses or strains: a tensile stress will determine an increase in the lattice spacing and, hence, a decrease in the wavenumber of the vibrational mode. In the case of compressive strain, the decrease of the lattice parameter yields a corresponding increase of the vibrational frequency. If the deformation of the structure follows an elastic behaviour, the shift will vary linearly with the magnitude of the stress, and as a result, the position of the Raman band can be used to measure the stress. It is well known that sharp Lorentzian band at 520 cm^{-1} of the first order Raman spectrum of crystalline silicon is quite sensitive to the presence of stress. For a biaxial stress in elastic regime, the stress ε in silicon can be obtained from:

$$\varepsilon = 250 \times \Delta\upsilon \text{ Mpa/cm}^{-1}$$

where $\Delta\upsilon$ is the Raman shift in wavenumber. Since the fabrication processes of semiconductors devices often produce strains in some localized microscopic regions, the Raman microprobe was found very useful in analyzing these microdomains. This technique is now recognized as a powerful tool in identifying stress and strain in polycrystalline silicon structures used for the fabrication of large polysilicon micromechanical structures [1-3]. These micromechanical systems based on surface-micromachining technologies can have serious stress effects that can cause mechanical device failure, curling or fracture, therefore, the micro-Raman system can be used as a quality control method and to improve several technological parameters.

Further, the presence of crystalline disorder also produces changes in the frequency of the band, usually towards lower wavenumbers. These are related to the breaking of translational symmetry in the crystal, which can be due to structural defects such as grain boundaries in nanocrystalline materials or dislocations. The position and shape of the Raman band can be simulated with a correlation length model [4] which allows to estimate the value of the correlation length L. L is defined as the characteristic size of crystalline domains where the translational symmetry of the crystal holds, and is related to the average grain size for nanocrystalline materials or to the average distance between defects for damaged crystals.

The presence of chemical impurities in the crystalline network may also give rise to changes in the mass of the atoms in the lattice sites which will shift the phonon frequency. For example, the presence of Ge atoms at substitutional positions in the silicon network produces a decrease in the frequency of the vibrational modes, due to a higher mass. This is known as the chemical effect and this has been used to characterize heteroepitaxial layers. For instance, the Raman spectrum of a typical $SiGe_x$ alloys, as shown in figure 1, presents three main lines, related to Si-Si at about 500 cm^{-1}, Si-Ge around 410 cm^{-1} and Ge-Ge about 290 cm^{-1} vibrational modes. The wavenumber of these modes follows a linear relationship with both chemical composition and strain [5]:

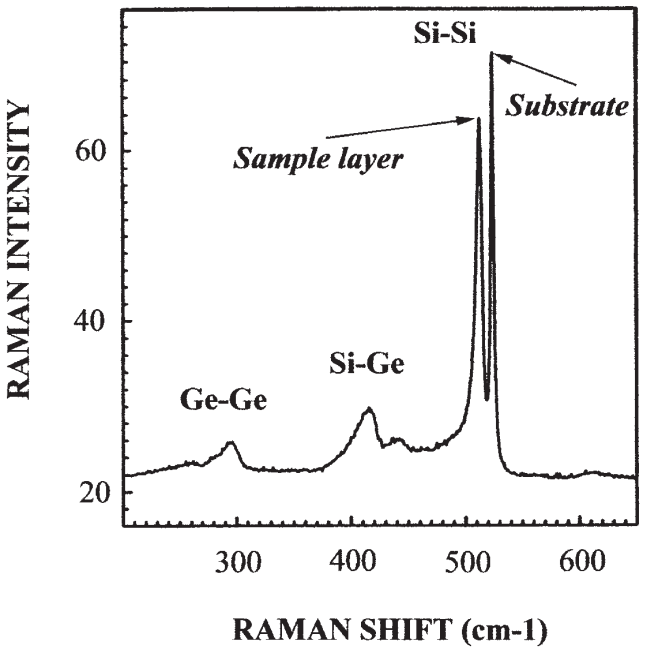

Figure 1. Raman spectrum of $SiGe_{0.3}$, showing the Si-Si, Ge-Ge and Si-Ge vibrational modes. The Raman band at 520 cm^{-1} is due to the crystalline Si substrate.

$$\upsilon_{\text{Si-Si}} = 520 - 68x - 830\sigma$$
$$\upsilon_{\text{Si-Ge}} = 500.5 + 14.2x - 575\sigma$$
$$\upsilon_{\text{Ge-Ge}} = 282.5 + 16x - 384\sigma$$

where υ is the wavenumber of the Raman mode, x the chemical composition and σ the strain parallel to the substrate. Using these relationships, a single Raman spectrum of $SiGe_x$ allows the determination of silicon and germanium contents as well as strain. Similar relationships have also been proposed for SiC_y as well as for more complex $SiGe_xC_y$ and $SiGe_xB_y$ ternary alloys [6,7].

Raman bandwidth

Raman bandwidth and bandshape are closely related to the crystalline order. In principle the bandwidth is related to the lifetime of the phonons. The presence of crystalline disorder produces a decrease of the phonon lifetime which thus generates an increase of the bandwidth. Therefore the density of defects can be evaluated from the bandwidth.

On the other hand, the bandshape of the Raman line is also affected by confinement of phonons being that given by the correlation length model. This model allows the estimation of both the correlation length L and the average stress. This is interesting when studying nanocrystalline materials since average grain size is given by L. The main limit for this measurement is that phonon confinement only occurs for sizes in the nanometric range (L < 20 nm for Si). The

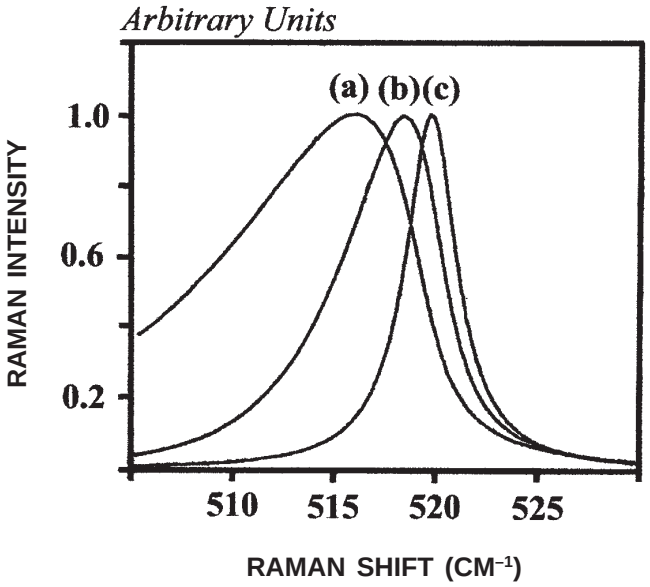

Figure 2. Simulation of the silicon first order Raman phonon mode assuming spherical confinement: (a) L = 60 Å, (b) L = 100 Å, (c) L = 200 Å.

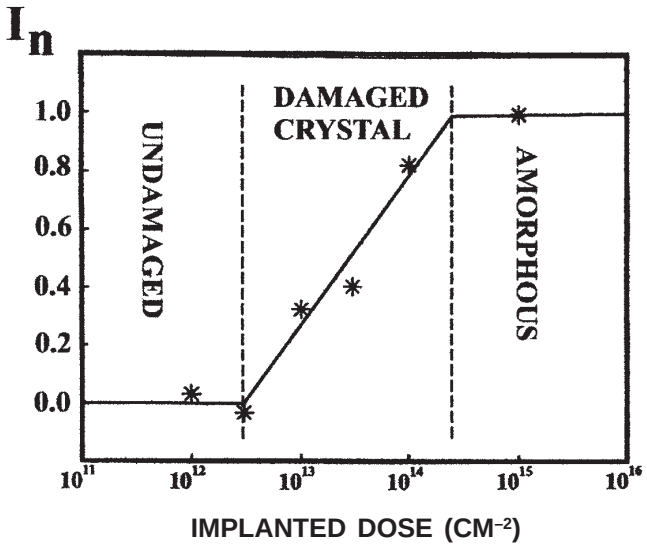

Figure 3. Relative micro-Raman intensity of the Longitudinal Optical mode of 6H-SiC versus the implantation dose.

changes in the bandshape and position of the Raman band related to phonon confinement has permitted the assessment of the average grain size and stress in nanocrystalline Si layers [8], as well as the density of defects in highly damaged Si films [9]. Figure 2 shows the spectra simulated for Si assuming spherical confinement and different values of the correlation length. As can be seen, for values of L below 20 nm, the Raman band is shifted towards lower frequencies and asymmetrically broadened, and both band shift and broadening increase as L decreases.

Raman intensity

The intensity of the Raman band is also very sensitive to the structure of crystals and as a result, significant information can be obtained from intensity measurements. Damage in the lattice leads to a decrease of the intensity of the first order modes, related to the breaking of bonds and changes in atomic forces displacements, and, hence produces a decrease of the Raman polarizability tensors. For instance, typical ion bombardment during doping process will alter the original crystal with a consequent reduction of the Raman signal intensity. The measurement of the Raman band intensity has therefore been applied to quantify the residual damage in processed wafers, such as ion implanted structures. Figure 3 shows an example on the quantification of the implanted induced damage in wafers of 6H-SiC (an hexagonal polytype of SiC) implanted with different doses of Ge^+ ions [10]. This is determined through the normalised intensity $I_n = (I_o - I)/I_o$, where I is the intensity of the Raman band measured in the implanted layer and I_o is the intensity of the Raman band measured in a virgin non processed sample. For a low degree of damage, I is very similar to I_o and I_n is close to 0. As damage increases, I decreases and I_n tends to the maximum value of 1. This last value gives a 100 % of damage, which corresponds, to the damage level for which fully amorphization of the implanted layer occurs. In this case, all the crystalline modes vanish from the spectrum, and I becomes 0. This method permits to check the degradation of the crystalline structure and is also used for optimizing annealing process after ion implantation in order to eliminate the induced damage.

Intensity measurement is also performed for quantitative analysis of different polymorphisms, defects, disorder, micro-inhomogeneities, etc. Micro-Raman mapping measurements can also be carried out in order to determine in a non destructive and simple way the thickness and structural uniformity of thin films, such as cobalt silicide films ($CoSi_2$) deposited on Si used for IR detectors technology [11]. This was obtained by measuring the intensity of the Raman signal from the Si substrate at different points on the surface. As can be seen in Figure 4, the intensity of the Raman line of the substrate decreases in an exponential way as the thickness of the layer increases. This is due to absorption of light in the layer. This method allows detection of $CoSi_2$ films as thin as 3-4 nm, and the $CoSi_2$ film thickness can be measured in the range between 10 and 100 nm with an uncertainty below 10 %.

Since the fabrication processes of semiconductors devices often produce strains in some localized region, a large amount of the micro-Raman studies were focused in identifying these micro-domains. Stress distributions and residual stresses have been determined in several semiconducting

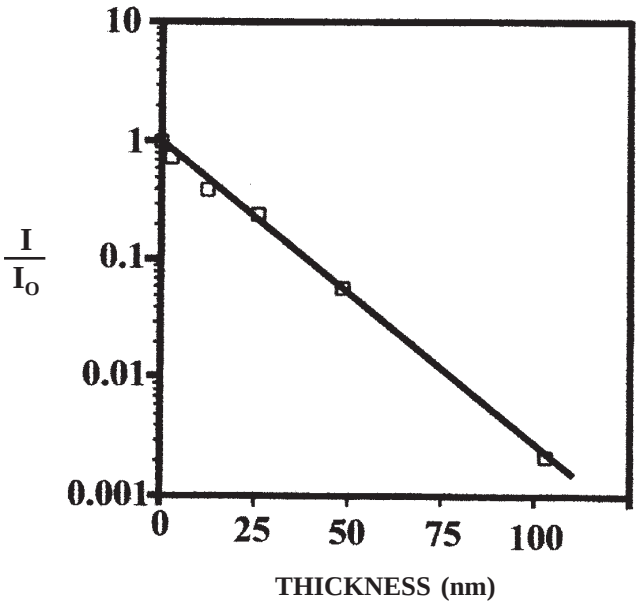

Figure 4. Relative Raman intensity of the first order Si mode in function of $CoSi_2$ thickness.

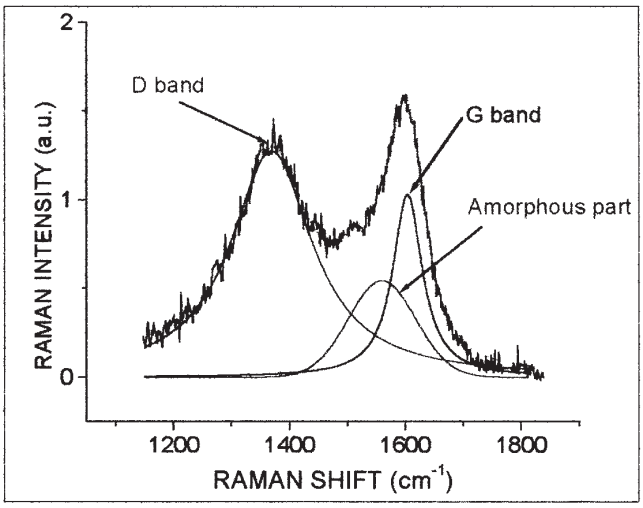

Figure 5. Micro-Raman spectrum of a single particle of black carbon with the corresponding curve fitted bands.

materials such as silicon implanted structures [12], polysilicon layers [13], local oxidation of silicon (LOCOS) structures [14], grooved devices [15], epitaxial and heteroepitaxial layers [16,17], semiconductor films grown on patterned substrates [18], etc.

Polarization Raman micro-analyses have also been carried out on semiconductors layers in order to examine local crystallographic orientation [19-20]. Micro-Raman spectroscopy is an interesting tool for determining the distribution of free electrical charge carriers concentration and mobility in III-V compounds, such as GaAs, GaP, GaAlAs, etc., without carrying out electric measurements using electrodes [21-22]. For highly doped p-type Si, the concentration of carriers can also be determined from the Fano-like deformation of the first order Raman line [6].

Information on local temperature in laser mirrors has allowed the optimization of device technology [23-24]. These were determined from the Stokes/anti-Stokes intensity ratio of Raman scattering. Finally, Raman microspectroscopy was used to study semiconductor microstructure fabrication by direct laser writing [25], evaluate change of the crystal quality in molecular beam epitaxial GaAs layers on Si [26], and identify contaminants in integrated circuits [27,28]. More applications of Raman microspectroscopy on semiconducting materials can be found in references 29, and 30.

In the research field of carbonaceous materials, micro-Raman spectroscopy is a fundamental tool for their characterization since the different polymorphs of carbons, such as diamond (sp^3) or graphitic (sp^2) structures, can be straightforwardly determined by the method. Further, the Raman signal is sensitive to short range disorder which allows the determination of the amorphous phase as well as crystals size. Figure 5 shows the micro-Raman spectrum of an individual black carbon particle. A curve fitting was carried out in order to determine with great accuracy the spectroscopic parameters such as peak position, bandwidth, lineshape and band intensity. The spectrum is formed of 3 bands: two bands D and G with a Lorentzian shape, at 1 370 and 1 603 cm^{-1}, respectively, and a broader Gaussian feature centered at about 1 550 cm^{-1} assigned to amorphous graphitic phase. The micro-Raman analysis shows that this material has a high degree of disorder and consists principally of non-hydrogenated sp^2 carbon bonds [31]. Further, the microcrystalline planar crystal size can be determined from the following relationship:

$$L_a = [I(D)/I(G)]^{-1}$$

where I(D) and I(G) are the integrated intensities of the D and G bands, respectively. As expected, the sample analyzed here has a low microcrystalline planar size, *i.e.* L_a is of the order of 2 nm.

Since many microstructural information can be obtained from the Raman spectra of carbons, Raman microscopy was found to be a very valuable method in characterizing new synthesized carbons-based materials [32-36] such as fullerene, fullerite, nanotubes, carbon fibers, layered intercalate carbon-based structures, etc.

One of the main advantages of Raman microspectroscopy when applied to thin films is that it can permit to detect in a non destructive way and rapidly small precursor compounds during the layer growth. This is quite important for thin films deposition technology since the characterization

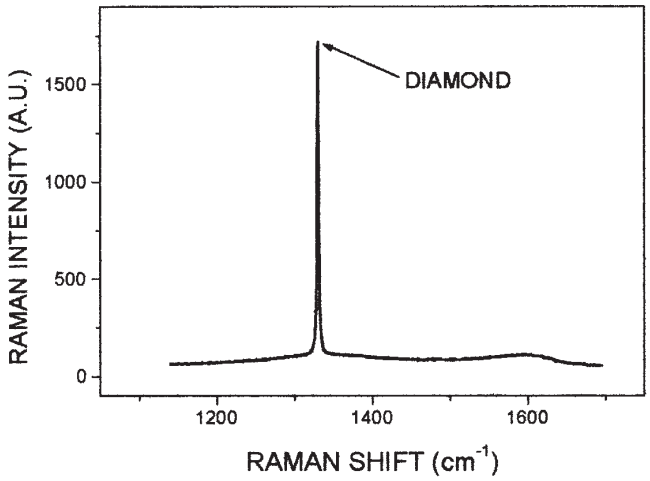

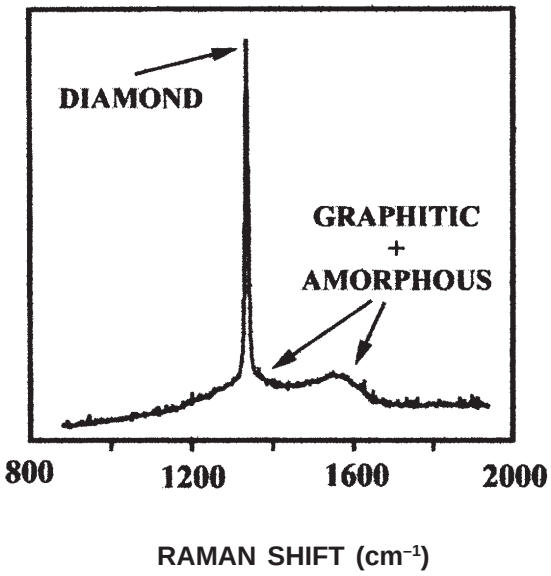

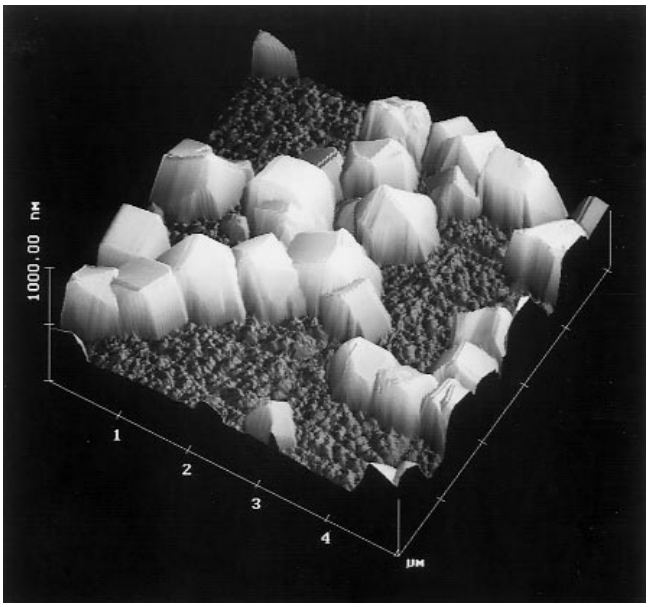

Figure 6(a). AFM micrograph of some precursor crystals with the Raman spectrum of one of these crystallites (Courtesy of M.C. Polo).

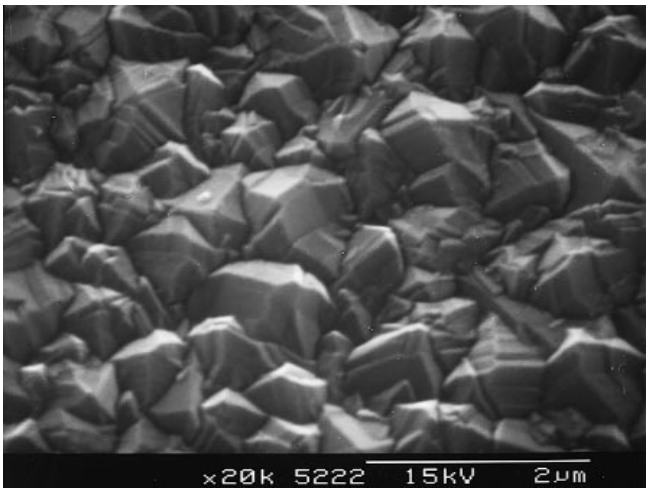

Figure 6(b). SEM micrograph of a CVD (Chemical Vapour Deposition) layer with its corresponding micro-Raman spectrum.

of these precursors, which often consists in small individual grains, allows to know if the processing conditions are correct or should be changed [37-38]. For example, the Raman spectrum of a single micro-crystal of figure 6(a) corresponds to that of a high quality diamond crystal whereas the spectrum of the thin film, shown in figure 6(b), indicates in addition of sp^3 carbons some degree of disorder and graphitic structures. The micro-Raman analysis of the layer presented in the figure 6(c) shows that the obtained thin film is mainly formed of highly disordered polycrystalline graphites as well as amorphous carbons.

The micro-Raman method was also used to follow *in situ* the kinetic of crystallization of hydrogenated nanostructured silicon (ns-Si:H) and hydrogenated amorphous silicon (a-Si:H) thin films obtained with a plasma enhanced chemical vapour deposition reactor. Figure 7 shows that the crystallization dynamics, as the laser power is increased, is higher for the nanostructure (ns-Si:H). This was explained by the fact that the nanostructured thin films is formed of small clusters that work as seeds for the crystallization process whereas in the case of the amorphous thin film (a-Si:H) higher energies are needed to start the nucleation [39]. The analysis of these spectra also permits the evaluation of crystals size and temperature.

Recently, the thin film technology was applied to the field of medicine and Raman microscopy was used to character-

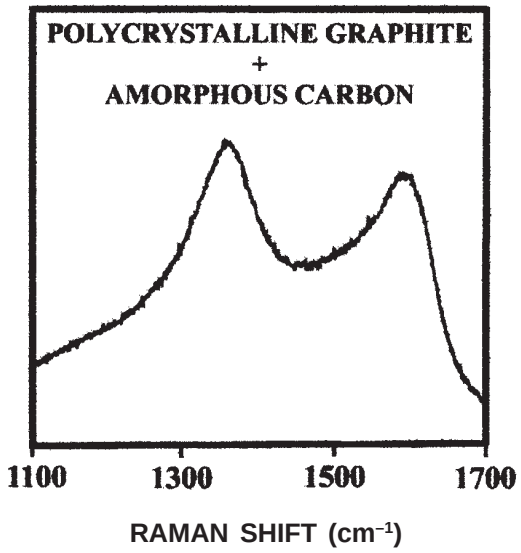

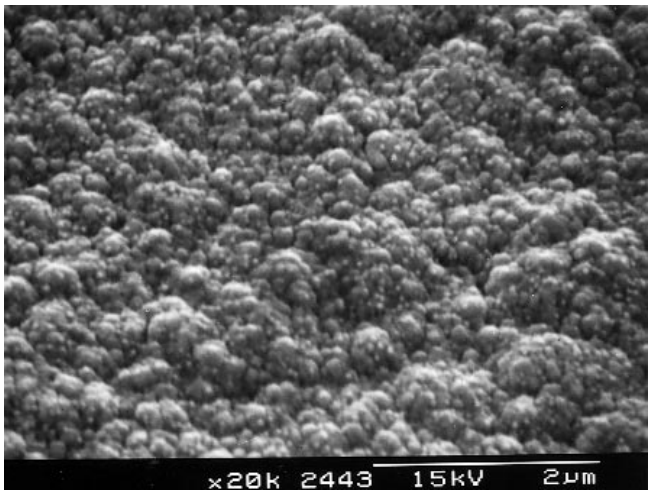

Figure 6(c). SEM micrograph of a different CVD layer with its corresponding micro-Raman spectrum.

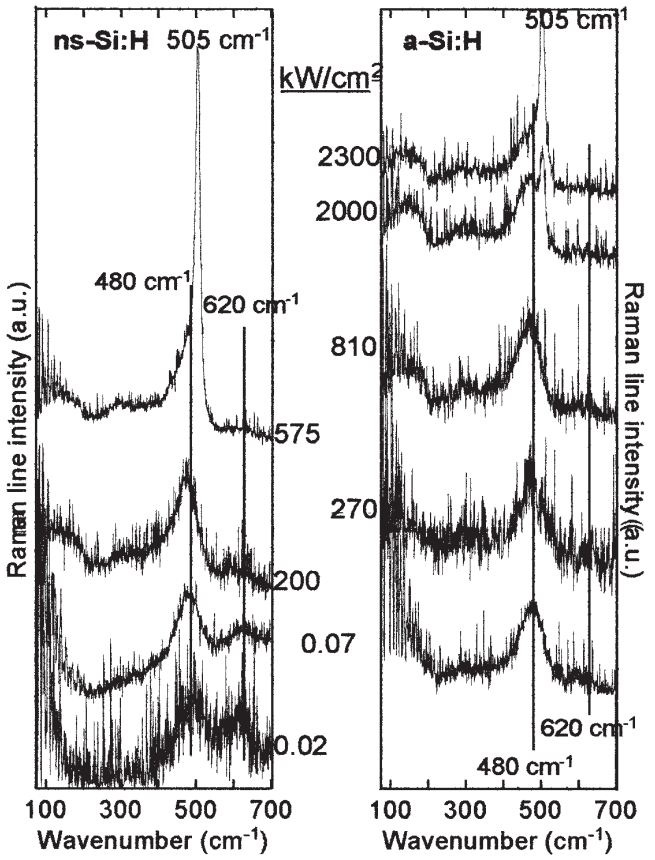

Figure 7. *In situ* evolution of the Raman spectrum of hydrogenated nanostructured silicon (ns-Si:H) and hydrogenated amorphous silicon (a-Si:H) thin films with the laser power density (Courtesy of G. Viera).

ize these new advanced layers: for instance thin films of hydroxyapatite ($Ca_{10}(PO_4)_6$ $(OH)_2$), which is a stable and osteoconductor material and thus a promising material for medical protesi, were obtained by laser ablation. Raman microscopy allows a rapid identification of the different calcium phosphates that may take place during the deposition process. In figure 8, in addition of hydroxyapatite (zone I), crystals of tricalcium phosphate ($Ca_3(PO_4)_2$), which is a material of lower quality for medical protesis, were detected in zone II with the Raman micro-probe. Whereas the separation between the two structures is relatively difficult by SEM, the micro-Raman analysis allows a clear distinction between the crystals of hydroxyapatatite and tricalcium phosphate. Therefore, micro-Raman spectroscopy can be straightforwardly utilized to follow and develop deposition processes of thin films for medical applications [40,41].

Conclusion

The examples presented here illustrate well the great possibilities that offers the micro-Raman technique for the characterization of the solid state. One of the main advantages of the method is that it allows to analyze specific localized micro-regions with no sample preparation. Micro-Raman spectroscopy not only permits the identification of the different materials at microscopic level but also provides a large variety of parameters related to the microstructure of the condensed state.

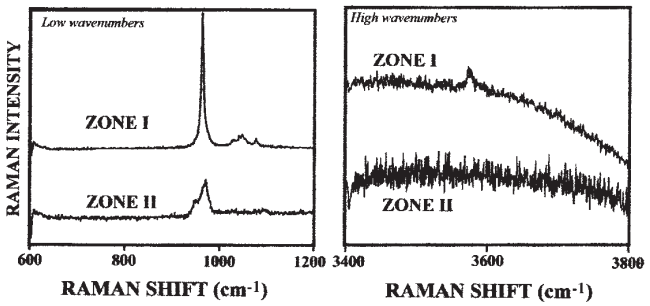

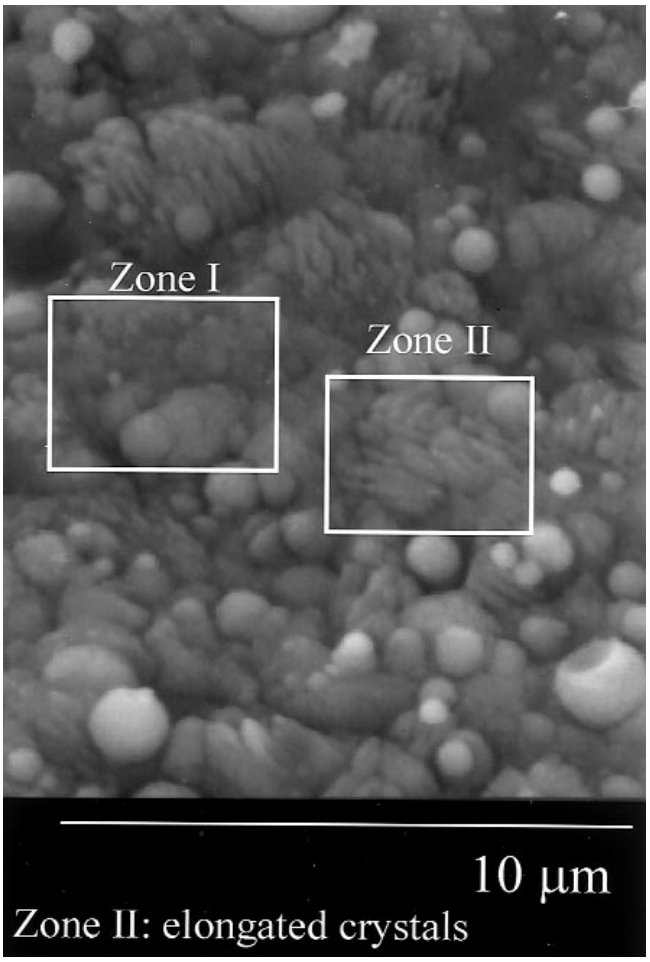

Figure 8. Micro-Raman spectra recorded in two different zones of a calcium-phosphate coating deposited by laser ablation with the corresponding SEM micrograph indicating the respective regions (Courtesy of L. Clèries).

References

1. Benitez, M.A.; Fonseca, L.; Esteve, J.; Benrakkad, M.S.; Morante, J.R.; Samitier, J.; Schweitz, J.A. *Sensor and Actuators* **1996**, *A54*, 718-723.
2. Morante, J.R.; Samitier, J.; Benrakkad, M.S. *Microelectronic J.* **1996**, *27*.
3. Furtsch, M.; Offenberg, M.; Vila, A.; Cornet, A.; Morante, J.R. *Thin Solid Films* **1997**, *296*, 177
4. Fauchet, P.M.; Campbell, H.I. *CRC Crit. Rev. Solid State Mater. Sci.* **1988**, *14*, S79.
5. Tsang, J.C.; Mooney, P.M.; Dacol, F.; Chu, J.O. *J. Appl. Phys.* **1994**, *75*, 8098.
6. Pérez-Rodríguez, A.; Romano-Rodríguez, A.; Cabezas, R.; Morante, J.R.; Jawhari, T.; Hunt, C.E. *J. Appl. Phys.* **1996**, *80*, 5736-5741
7. Pérez-Rodríguez, A.; Cornet, A. Morante, J.R. *Microelectronic Eng.* **1998**, *40*, 223-237.
8. Achiq, A.; Rizk, R.; Gourbilleau, F.; Madelon, R.; Garrido, B.; Pérez-Rodríguez, A.; Morante, J.R. *J. Appl. Phys.* **1998**, *83*, 5797.
9. Macía, J.; Martin, E.; Pérez Rodríguez, A.; Jiménez, J.; Morante, J.R.; Aspar, B.; Margail, J. *J. Appl. Phys.* **1997**, *82*, 3730.
10. Pérez-Rodríguez, A.; Pacaud, Y.; Calvo-Barrio, L.; Serre, C.; Skorupa, W.; Morante, J.R. *J. Electr. Mater.* **1996**, *25*, 541.
11. Pérez-Rodríguez, A.; Roca, E.; Jawhari, T.; Morante, J.R.; Schreutelkamp, R.J. *Thin Solid Films* **1994**, *251*, 45-50.
12. Macía, J.; Jawhari, T.; Pérez-Rodríguez, A.; Morante, J.R. *The Electroc. Soc. Proc.* **1994**, *94*(11), 148-153.
13. Benrakkad, M.S.; Pérez-Rodríguez, A.; Jawhari, T.; Samitier, J.; López-Villegas, J.M.; Morante, J.R. *Mater. Res. Soc. Symp. Proc.* **1994**, *343*, 609-614.
14. Vanhellemont, J.; De Wolf, I.; Janssens, K.G.F.; Frabboni, S.; Balboni, R.; Armigliato, A. *Appl. Surf. Sci.* **1993**, *63*, 119.
15. Hashimoto, A.; Kamijoh, T.; Watanabe, N. *Japan. J. Appl. Phys.* **1987**, *26*, L1128.
16. Rothwell, W.J.; Davey, S.T.; Wakefield, B.; Gibbings, C.J.; Tuppen, C.G. *Inst. Phys. Conf. Series* **1989**, *100*, 253.
17. Ilzuka, K.; Yoshida, T.; Matsuda, I.; Hirose, H.; Suzuki, T. *Mater. Sci. Engin.* **1990**, *B5*, 261.
18. Tang, W.C.; Rosen, H.J.; Guha, S.; Madhukar, A; *Appl. Phys. Lett.* **1991**, *58*, 1644.
19. Kolb, G.; Salbert, T.; Abstreiter, G. *J. Appl. Phys.* **1991**, *69*, 3387.
20. Mizoguchi, K.; Nakashima, S. *J. Appl. Phys.* **1991**, *65*, 2583.
21. Nakashima, S.; Yugami, H.; Fujii, A.; Hangyo, M.; Yamanaka, H. *J. Appl. Phys.* **1988**, *64*, 3067.
22. Herms, M.; Irmer, G.; Monecke, J.; Oettel, O. *J. Appl. Phys.* **1992**, *71*, 432.
23. Abstreiter, G. *Appl. Surf. Sci.* **1991**, *50*, 73.
24. Tang, W.C.; Rosen, H.J.; Vettiger, P.; Webb, D.J. *Appl. Phys. Lett.* **1991**, *58*, 557.
25. Herman, I.P., Magnotta, F. *J. Appl. Phys.* **1987**, *61*, 5118.
26. Ito, A.; Ichimura, M.; Usami, A.; Wada, T.; Kano, H. *J. Appl. Phys.* **1992**, *72*, 2531.
27. Hiratsuka, Y.; Hirano, Y.; Tochigi, K. *Mikrochimica acta* **1984**, *3*, 359.
28. Muggli, R.Z.; Andersen, M.E. *Solid State Tecnol.* **1985**, *28*, 287.
29. Jawhari, T. *In: Handbook of Advanced Materials Testing* (N.P. Cheremisinoff Ed.); Marcel Dekker: New York, 1995, 105-144.
30. Jawhari, T.; Pérez-Rodríguez, A. *The Internet Journal of Vibrational Spectroscopy* **1999**, *II*(4), 41-82 (http://www.ijvs.com/volume2/edition4/ section1.htm).

31. Jawhari, T.; Roig, A.; Casado, J. *Carbon* **1995**, *33*, 1561-1565.
32. Afanasyeva, N.I.; Jawhari, T.; Klimenko, I.V.; Zhuravleva, T.S. *Vibrat. Spectrosc.* **1996**, *11*, 79-83.
33. Klimenko, I.V.; Zhuravleva, T.S.; Jawhari, T. *Synth. Met.* **1996**, *86*, 1-3.
34. Afanasyeva, N.I.; Belogorokhov, A.I.; Blank, V.D.; Jawhari, T.; Ovchinnikov, A.A. *Macromol. Symp.* **1997**, *119*, 207-212.
35. Klimenko, I.V.; Zhuravleva, T.S.; Afanasyeva, N.I.; Jawhari, T. *Polym. Sci. A* **1996**, *12*, 1336-1342.
36. Klimenko, I.V.; Zhuravleva, T.S.; Geskin, V.M.; Jawhari, T. *Mater. Chem. Phys.* **1998**, *56*(1), 14-20.
37. Polo, M.C.; Cifre, J.; Sánchez, G.; Aguiar, R., Varela, M.; Esteve, J. *Appl. Phys. Lett.* **1995**, *67*, 485.
38. Polo, M.C.; Wang, W.L.; Sánchez, G.; Andújar, J.L.; Esteve, J. *Diamond Relat. Mater.* **1997**, *6*, 579.
39. Viera, G.; Roca, P.; Costa, J.; Martínez, S.; Bertran, E. *Mat. Res. Soc. Symp. Proc.* **1998**, *507*, 933-938.
40. Clèries, L.; Fernández-Pradas, J.M.; Sardin, G.; Morenza, J.L. *Biomaterials* **1998**, *19*, 1483-1487.
41. Fernández-Pradas, J.M.; Sardin, G.; Clèries, L.; Serra, P.; Ferrater, C.; Morenza, J.L. *Thin Solid Films* **1998**, *317*, 393-396.